Damage of bearings caused by electrical discharge currents at large drives derived from latest field research results

Dipl.-Ing. (FH) Sven Tröger [1], Prof. Dr.-Ing. Matthias Kröger [2]

[1] *Institute for Machine Elements, Design and Manufacturing, Technische Universität Bergakademie Freiberg, sven.troeger@imkf.tu-freiberg.de*
[2] *Institute for Machine Elements, Design and Manufacturing, Technische Universität Bergakademie Freiberg, Kroeger@imkf.tu-freiberg.de*

Abstract

Bearing currents are not all the same. Under certain circumstances and special use cases classic bearing insulations are not sufficient anymore to prevent bearing currents due to the operation of frequency converters. Additional corrective measures have to be implemented to reduce the source of bearing currents the common mode current. The usage of nanocrystalline tape wound cores shows high effectiveness. As part of a big field study with more than 50 large drive trains in the primary industry, the damaging mechanics of bearing currents are examined under real conditions. Of exceptional high interest is the influence of disturbances which can hardly be simulated in the laboratory. Additional to the shielded motor cable parallel installed functional potential equalization cables applied multiple times have almost no effect in regard to reducing the bearing current. With an optimal installed functional potential equalization system more than 95 percent of the common mode current can flow back through the motor cable shield to the converter. The disturbance impact in the field can influence the voltage over the bearing that breakthroughs are favored but also reduced.

Keywords – electrical discharge currents, EDM, bearing currents, common-mode current, tape wound cores

1 Introduction

Current frequency converters and electrical motors of numerous manufacturers are characterized by a high control quality and an increasing optimization regarding power loss and energy efficiency. Their products become more and more productive and capable. In an industrial environment mainly frequency converters with insulated gate bipolar transistors (IGBT) are used. Due to this technical development the voltage rise times of the single pulses are very short and therefore exceptionally sharp voltage edges with high peaks of the pulse-width modulated motor terminal voltage are observed through all manufacturers. These voltage peaks of the converter phases and their harmonics do not add up to zero in contrast to a classic three-phase sinus

network. A common-mode voltage against earth remains. Conditioned by the constructive internal capacities of the motor, this common-mode noise voltage drives an unwanted high frequent interfering current named common-mode current. The common mode voltage is divided by the internal capacities according to the following ratio of the so-called Bearing Voltage Ratio (BVR) [1],

$$BVR = \frac{bearing\ voltage}{common\ mode\ voltage\ stator}, \quad \text{(Eq. 1-1)}$$

$$BVR = \frac{U_B}{U_{CM}} = \frac{C_{WR}}{C_{WR}+C_{RF}+2C_B}. \quad \text{(Eq. 1-2)}$$

It is the relation of the common-mode voltage (U_{CM}) at the motor terminal to the voltage (U_B) at the rolling bearing. Therefore, the motor forms by intern capacities a capacitive voltage divider. The essential capacities are the capacity winding stator to rotor C_{WR}, the rotor to frame capacity C_{RF} and the bearing capacities C_B (fan side NDE and drive side DE), cp. Figure ***3-1***. To avoid bearing damage by current flashover in the bearing the pending voltage at the bearing should be as low as possible. Various investigations show that even small voltages in the single digit range may lead to damage by electrical discharge currents in the bearing of a motor [2], [3]. At low voltages the grease in the contact surface between rolling elements and bearing raceway can insulate and prevent discharge. How high the voltage at the bearing is in reality depends on numerous factors. At almost identical drive trains very different bearing voltages and common-mode currents can be observed many times.

2 Bearing currents in praxis

In the past years many studies have been focused on the topic of bearing currents in the laboratory. By now many relations regarding origin and influence of bearing currents are well known and can partly be simulated. Very detailed research results and fundamentals give [1], [4], [5], [6], [7], [8], [9], [10]. In the heavy industry with real large drives in megawatts it is very hard to confirm the measurement series from the laboratory in detail. This derives from the limited possibilities to prepare the motor in the field and also mainly by the large number of disturbances and variables influencing the bearing currents and measurement series.

Furthermore, effects triggered by the disturbance variables lead to new aspects and understanding of bearing currents.

2.1 Damage pattern

The typical damage pattern of bearing currents shows significant axially parallel marks so-called ripples at the inner and outer runway. Figure ***2-1*** shows a noticeable damaged fan side rolling bearing of a 800 kW low-voltage motor in an industrial use as a multi-motor drive after a runtime of 4 years. The outer ring of the bearing is galvanically insulated by a ceramic coating towards the bearing seat of the motor. Despite this insulation bearing currents can be observed. This distinguishes classic bearing current problems which are known since a long time from current problems in the industry. The "new bearing currents" overcome the effective insulation in contrast to classic low frequent bearing currents by capacitive coupling. Thereby the ceramic coating serves as dielectric between the metallic bearing seat and the bearing outer ring of the motor. If current flows through the bearing and breaks through the insulating bearing grease typically via the rolling elements from one ring to the other ring damages occur. The process at the contact surfaces is similar to the electrical arc welding. The runway material heats up and reaches temperatures which lead to hardening or melting [2]. The results are discolored areas of different size in which the material is annealed (heated below melting point), cured or melted. In areas where the metal is melted cratering can be observed [2], [4]. Direct current as well as alternating current may lead to bearing damage. Even currents with low amperage can cause damage. The degree of damage depends on many factors. Mainly on amperage, duration and amount of applied bearing voltage, number of flashovers, bearing load, bearing speed, bearing temperature and grease characteristics [1], [4].

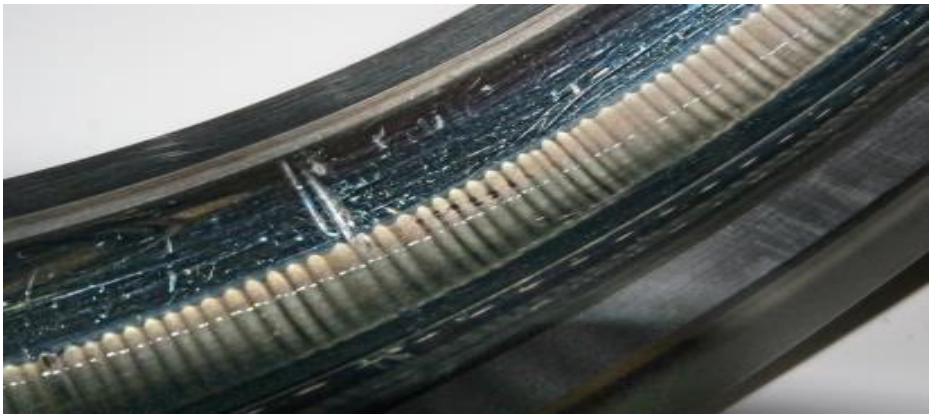

***Figure 2-1**: Macroscopic photography of a rolling bearing surface with electrical discharge erosion marks, 800 kW motor.*

Preliminary to the ripple forms a typical matting of the runways is observed. The matting also affects the rolling elements. The oblique light microscopic image (Figure ***2-2***) shows the spreading of the individual melting craters of the bearing runways which make the otherwise metallic reflecting surface seem matt. A high concentration of the craters in the ripple-shaped appearing parallel parts can be seen. A matting of the surface without ripple shaping can thereby exist without damage of the rolling characteristics and the effective bearing vibrations.

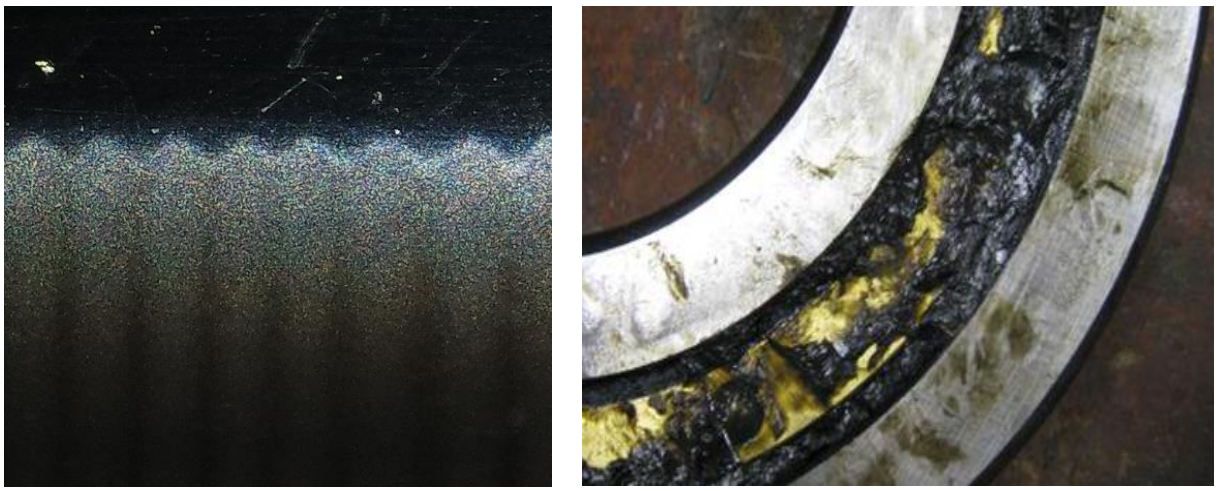

***Figure 2-2**: Oblique light microscopic analysis of the electrical discharge erosion marks (each visible pixel is one mark), (left).*

***Figure 2-3**: Burned grease of a damaged bearing by bearing currents after 40.000 operating hours (right)*

As a result of the electrical discharges the grease gets heated in the area of the breakthrough tunnel and burns at this points. Due to this and the input of wear material the grease is dark

brown or black instead of the turquoise colored in its original state, which is just one more evidence of the presence of bearing currents, see Figure 2-3.

In course of the research the grease of 35 bearings was laboratory diagnostically analyzed. For reference all measurements were also performed with fresh grease of the brand Shell-Gadus S2. This grease type was used in the examined rolling bearings.

The results of the grease analysis (Table ***2-1***) show a significant increase of the iron part in comparison to the new grease. In connection to the listed PQ-Index this points to an increased wear. The PQ-Index gives evidence of the total quantity of magnetized iron parts (parts > 5 µm) in the grease which arise from the damage pattern. Increased copper values result here from the wear of the brass cage.

Table 2-1*:Laboratory diagnostical grease analysis of bearing current damaged bearings.*

Extract of a typical grease sample	New reference grease Shell-Gadus S2	Grease sample after 40.000 h	
		Drive end	Non-drive end
Iron [ppm]	0	2505	1712
Chromium [ppm]	0	26	15
Copper [ppm]	0	320	4
PQ-Index [ppm]	o.k.	117	106
Bleeding test, oil loss [wt. %]	28	10	15

The determined values of the bleeding test give evidence of the residual oil content of the grease and therefore of the lubricity. The lubricity of the bearing can be confirmed. Is the value in the range of 10 the grease is limited capable to emit the oil needed to lubricate the bearing. All examined samples were still limited lubricative despite strong visual aging.

2.2 Influence and disturbance variables of bearing currents

Meanwhile a large number of influence variables are known having an impact on bearing currents. The majority of the following listed factors can only limitedly be influenced in the real industrial environment or rather kept constant.

Especially the following influence and disturbance variables are to be expected ([1], [4], [5], [6], [7], [8], [9], [10]):

- Drive speed
- Dynamic operation mode, continuous ramp-up and ramp-down, change of direction

- Converter infeed controlled or uncontrolled
- Inner capacity of the motor (highly dependent on shaft height)
- Cable capacity
- Bearing load (axial, radial)
- Bearing construction: number of rolling elements, bearing capacity, load and position of the bearing
- Bearing insulation
- Bearing temperature
- Long service in creep velocity
- Cable length
- Motor cable: type, cable length
- Mechanical vibration caused by the motor or extern sources
- Motor cable type
- Network configuration: IT network, TN network
- Low impedance equipotential bonding
- Equipotential bonding by motor shaft: shaft scrubber, insulated coupling
- Grease characteristics: viscosity, conductivity, insulation capacity, aging resistance, bleeding, additives, transition of metals from the bearing
- Frequency of the voltage modulation
- Voltage level: 400 V, 690 V
- Intermediate circuit voltage
- Asymmetries: motor cable, winding of the motor
- Distortion of the network voltage, interferences of external disturbance variables of other plant sections

3 Origin and flow paths of common-mode voltages and currents in industrial plants as source of bearing currents

The following presented measurement series are all recorded from drivetrains used in the heavy primary industry. The examined factories distinguish with highly distorted IT networks and high parts of variable speed drive loads and main power cords greater than 20 MW.

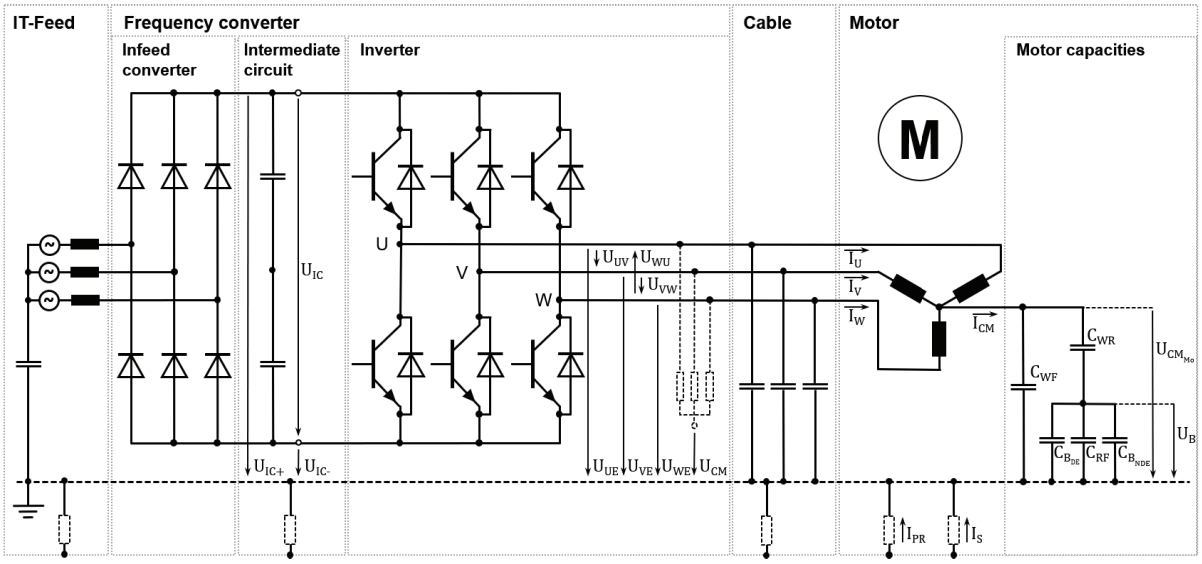

***Figure 3-1**: Overview of drive train*

Since the common-mode voltage is a voltage against earth potential it is even more important at all measurement series to investigate the voltage against earth to better understand the connections. All examined drives are equipped with an insulated non-drive end rolling bearing.

3.1.1 Rectification of the mains voltage

To get a variable-speed control of the motor in most cases a pulse width modulation is used to control the motor voltage. Therefore in a first step the sinusoidal mains power has to be rectified. The rectification can be done uncontrolled by diode bridges as well as controlled by insulated gate bipolar transistors (IGBTs). Beneficial for multi-motor drives are controlled feed-in converters due to the by stable DC intermediate circuit voltage by pulse width modulation and the fed back option at decelerating processes of the drives. Under field conditions the created DC voltage looks much distorted at the positive (U_{IC+}) and negative (U_{IC-}) connection points as shown in the Figure ***3-2***. Due to the only capacitive link of the 690 V IT networks against ground this effect is even increased. The momentary values oscillate between +/- 1,5 kV per signal.

The intermediate circuit voltage (U_{IC}) deriving from the potential differences at the positive and negative pickups is very stable due to the controlled infeed despite load variation at 1060 V. But this voltage is overlapped by very sharp and short peaks of up to 100 V_{pp}.

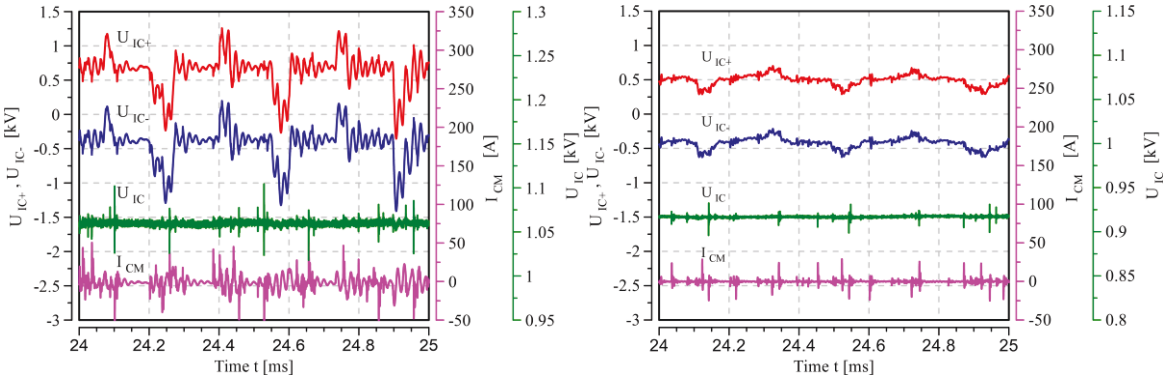

***Figure 3-2**: Controlled infeed, intermediate circuit voltage with strong distortion against ground (left)*

***Figure 3-3**: Uncontrolled infeed, intermediate circuit voltage with low distortion against ground (right)*

The systemic influence of the selection of the feeder converter can be seen in the comparison to the uncontrolled infeed (Figure ***3-3***). The measurements were recorded under the same network conditions in the same plant.

The examined uncontrolled diode bridge infeed features much less oscillation of the intermediate circuit voltage (U_{IC+}, U_{IC-}) against ground. Also much lower peak voltages of the intermediate circuit voltage (U_{IC}) smaller than 50 V_{pp} can be seen. The higher peaks are to be connected to the downstream output inverters. Nevertheless the circuit feedback on the upstream network due to increased reactive power demand and uneven harmonic waves has to been put in account at this infeed variant [4]. By a comparison of the flowing common-mode currents (I_{CM}) in the downstream motor to converter mesh, significant differences in the signal shape can be seen. At the controlled infeed the single common-mode current peaks are connected with rounded signal paths. Whereas at the uncontrolled infeed these roundings are missing. The individual peaks are well separated from the remaining signal path.

3.1.2 Modulation motor voltage

From the intermediate circuit voltage as the source a square wave voltage is generated by pulse width modulation in the inverter unit of the frequency converter on all 3 motor phases.

By the strong distortion against ground it can only be guessed from Figure ***3-4*** that the output from the inverter unit (motor phase voltages to ground: U_{WE}, U_{VE}, U_{UE}, phase-ground voltages) modulate a sinusoidal motor current.

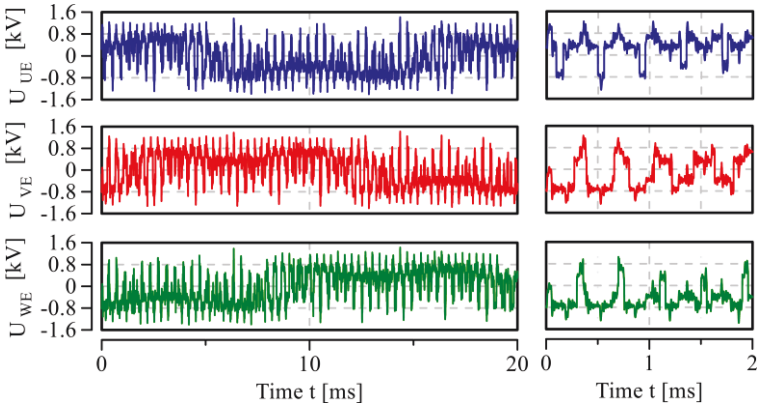

***Figure 3-4**: Motor phase voltages to ground (U_{UE}, U_{VE}, U_{WE}) at the inverter output*

The peak-peak phase voltages are in this case at the examined 690 V frequency converter up to 2.57 kV and show high-frequency components. All capacities to earth, especially the cable capacity and motor capacities can be transferred by these voltages, with the consequence of unwanted common mode currents. Also all insulating arrangements of the windings and voltage-carrying components of the engine must have sufficient insulation preparations against these high voltages. Otherwise there can be electrical discharges and breakthroughs of the windings against the grounded conductive motor housing.

If the motor phase voltages are compared side by side with respect to motor windings as chained voltages (U_{UV}, U_{VW}, U_{WU}) the almost perfect rectangular signal characteristics of the inverter modulation is shown. The meshed phase voltages arise as follows:

$$U_{UV}=U_{UE}-U_{VE},$$
$$U_{VW}=U_{VE}-U_{WE}, \qquad \textit{(Eq. 3-1)}$$
$$U_{WU}=U_{WE}-U_{UE}$$

The transistors of the inverter module switch the intermediate circuit voltage between two switching states $-U_{IC}$, $+U_{IC}$. From the formation of a fictitious center point the meshed voltages can get three levels $-U_{IC}$, $+U_{IC}$ und 0.

At the switching edges (Figure **3-5**) of the square wave signals high voltage rises can clearly be examined (here measured at the inverter output). Reflections can also be found at the motor winding. Corresponding peaks at the switching edges are visible on the motor phase current (I_U). These peaks result from reflections of the voltage signals at junctions of the motor cable with different shaft impedances [11]. As part of the field measurements very large differences in the amount of reflections and other capacitive couplings lead to ring vibrations.

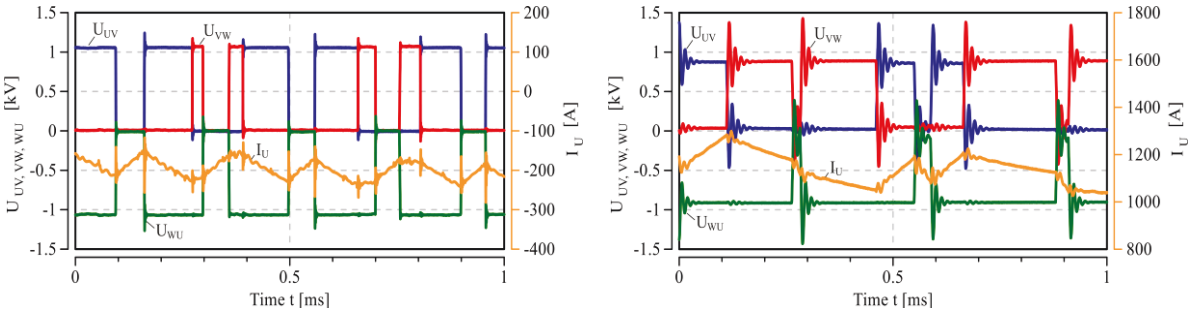

Figure 3-5*: Phase voltages of the inverter output with low reflections at switching edges of a multi-motor drive (left)*

Figure 3-6*: Chained voltages at the inverter output with strong reflections and resonances at capacitive switching flanks of a 800 kW, 690 V single drive (right)*

In comparison to the low classifiable reflections and capacitive ring vibrations in the first example (Figure 3-5), the following measurement (Figure ***3-6***) of an 800 kW, 690 V drivetrain shows that these effects can be much more pronounced depending on the cable capacity, motor capacity, impedances, and other factors.

3.1.3 Formation of the common mode voltage and the resulting common mode current

The common mode voltage (U_{CM}) and driven by this voltage the common mode current are the primary cause of the classic bearing current damage to drives, which are already protected against traditional bearing currents by bearing insulation and other design measures. The common mode voltage is the source of the capacitive voltage divider of rolling bearings according to the Bearing Voltage Ratio.

The common mode voltage forms in this process as a voltage of an imaginary neutral point of the phase-ground voltages (U_{UE}, U_{VE}, U_{WE})) with respect to ground (cp. Figure ***3-1***). The voltage can be calculated as follows

$$U_{CM} = (U_{UE} + U_{VE} + U_{WE}) / 3 \qquad \textit{(Eq. 3-2)}$$

Due to the described limited combinatorial switching states of the transistors of the inverter a very characteristic stepped common-mode voltage can be observed (U_{CM}).

The illustration Figure ***3-7*** shows an almost ideal step-shaped course of the common mode voltage and the resulting current (I_{CM}). This field measurement was taken on a 90 kW, 400 V multi-motor drivetrain with all other engines of the plant shut down, so almost no interferences from the plant network were present. Clearly can be seen that with potential change of the common mode voltage the capacity in the motor and motor cable reload. The resulting reversal current represents the common mode current (I_{CM}).

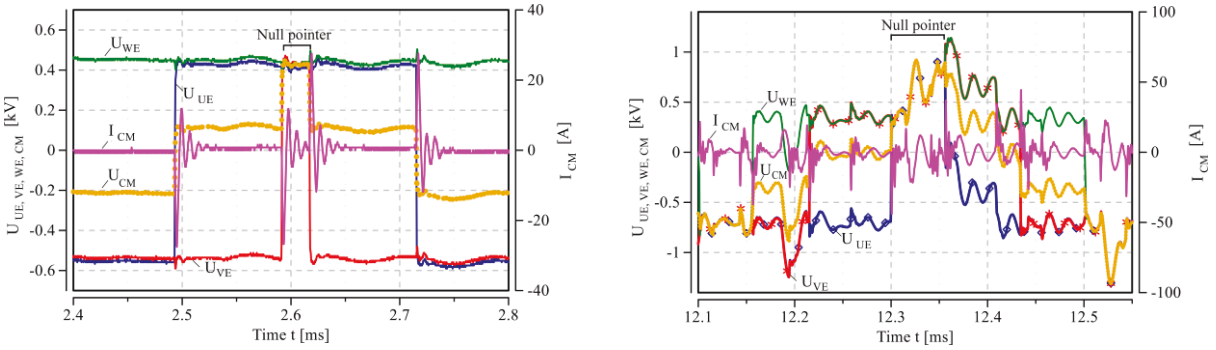

***Figure 3-7**: Stepped common-mode voltage, 90 kW drive, 400 V, uncontrolled diode bridge infeed, low disturbance factors (left)*

***Figure 3-8**: Distorted common-mode voltage, 335 kW drive, 690 V, regulated power supply, high disturbance factors (right)*

Since the common mode current peaks occur on the flanks of the changing common-mode voltage and discharge currents, current peaks are very short and have a high frequency. The maximum amount of the common mode voltages can be achieved in the second state when all three phase-to-ground voltages are switched to the positive or negative potential of each intermediate circuit voltage. This is the so-called null pointers [12].

Carrying out the same series of measurements on a multi-motor drive with further active inverter units on the same intermediate circuit voltage and regulated infeed a clearly different measurement result is observed, see Figure ***3-8***.

The common mode voltage is already between the switching edges of the IGBTs of the drive strongly rippled and distorted. The phase ground voltages are reasons for this. Due to the shared intermediate circuit voltage these show peaks of other inverters. Regulated infeed adds distortion to ground.

The resulting common-mode current thus has a number of other peaks which are not attributable to the switching edges of the phase-ground voltages of this drivetrain. Nevertheless these common-mode voltages and common-mode currents flow through the internal capacities in the motor and partly the rolling bearings. A relationship can clearly be identified between the peak frequency of the common mode current to the used infeed (controlled, uncontrolled) and a shared intermediate circuit with other drives.

3.1.4 Flow paths of common mode voltage and current on the potential compensation system

A large number of measurements has shown that for a well-functioning potential equalization system, which is of low impedance for frequencies of at least 500 kHz, more than 95 % of the common mode current (peak value) flows directly over the screen of the motor cable back to the frequency converter. Especially cables of the type NYCWY turned out low impedant besides special EMC cables which were used in all studies presented here. In NYCWY power cables the conductors are arranged concentrically and surrounded in total of a coaxial coarse wiry shield braid. The Figure ***3-9*** shows exemplary the return flow of common mode current (I_{CM} = 100,5 A $_p$), via the motor cable shield (I_S = 97,14 A $_p$) and the current flowing in the parallel to the motor cable extra fine braided parallel return conductor (I_{PR} = 2,1 A $_p$) of a 335 kW drivetrain in the field with controlled infeed. It can be clearly seen that while the common mode current on the outer conductor is almost identical in shape and size to reflux over the motor cable shield. The return on the parallel return line is very low. Typical to the backflow in the parallel return line is an overlay of additional low-frequency (from the field), which do not have the common mode voltage source. Due to the strong disturbance factors the ideal stepped common-mode voltage can only be guessed.

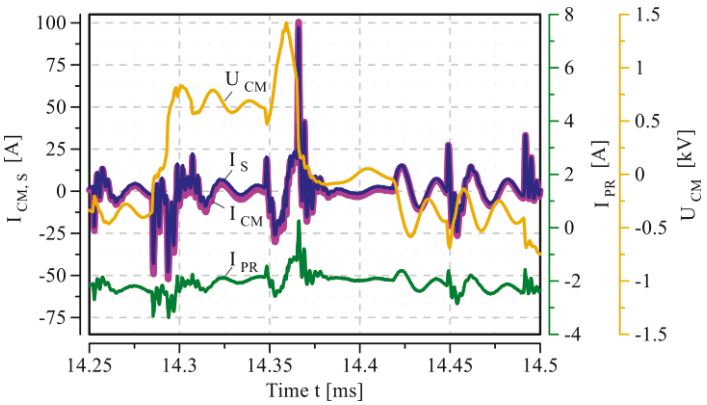

Figure 3-9*: Returns common mode current via motor cable screen and parallel return line, 335 kW drive, 690 V, IT network, controlled supply, strong disturbance factors*

3.1.5 Pending common-mode voltage on rolling bearings

The ratio of the voltage applied to the rolling bearing can be calculated by the described Bearing Voltage Ratio (BVR). In the field the voltage applied via the bearing can usually only be measured in motors with insulated bearing inserts. Here you can measure the voltage potential of the bearing outer ring to ground via the electrically conducting grease tube leading directly to the

outside without any preparations to the engine. The potential of the inner ring can be tapped via the motor shaft *($U_{S\,NDE}$)*. The potential difference of these two measured signals corresponds to the bearing voltage on the fan-side bearing ($U_{B\,NDE}$). Basically three different bearing currents have to be named, the circular current, rotor-earth current and EDM current. These are described in detail in [4]. The bearing current can flow capacitively through the bearing (grease insulates), resistively (no insulation effect in grease) or through breakthrough in the grease.

Figure ***3-10*** shows the voltage and current ratios on the fan side bearings of an 1150 kW drive. Before an EDM discharge in form of an arc takes place through the grease a voltage rise over the bearing ($U_{B\,NDE}$) can be observed.

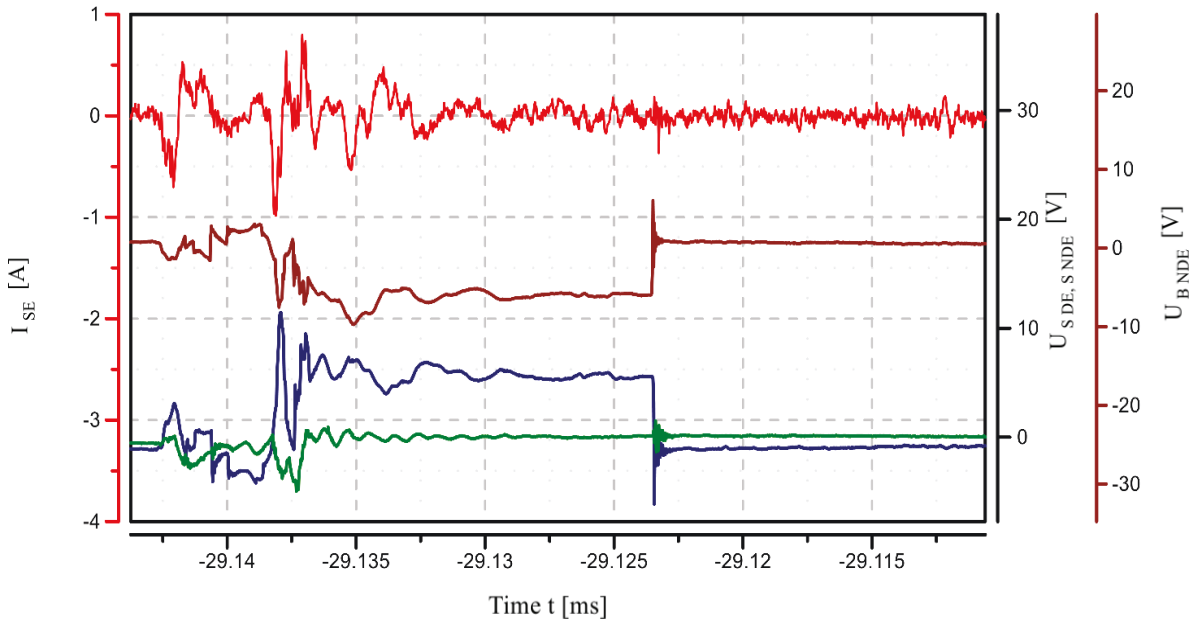

Figure 3-10*: Shaft voltages on the drive side ($U_{S\,DE}$, green) and the fan end ($U_{S\,NDE,}$, blue), as well as bearing voltage across the fan side rolling bearing (U_{B} NDE) and the rotor-ground current (I_{SE}), 1150 kW drive, 690 V, IT network, uncontrolled infeed, medium disturbance factors*

If the insulation capacity of the bearing grease is exceeded, there is a breakthrough through the grease and thus an arc discharge, which leads to the typical damage described between the contact surfaces. It can be observed that the voltage across the bearing frequently pends a few microseconds before it breaks [4].

Under field conditions and the influence of disturbances it shows that the bearing voltage follows the step-like ever-changing common-mode voltage and its distortion. Therefore, the bearing voltage is similarly high-frequent as the common-mode voltage. Very fast switches of polarity show with steep positive and negative edges. The flanks do not explicitly all show an

EDM breakthrough in the bearing. More often, these voltage curves are caused by capacitive coupling paths or by resistive couplings. Even without arc discharge respective peaks can be detected in the rotor-ground current. At the present investigated drive most small discharges look like the sample at -29.126 ms show up. The bearing voltage *(U B NDE)* breaks down suddenly to 0 V and a compensating current flows as shaft-ground current (*I SE*).

4 Frequencies in the drive train

In order to define appropriate protective measures against bearing currents damaging voltages and currents must be characterized accordingly. As the studies in the time domain show most signals have high-frequency components, otherwise the capacitive coupling mechanisms would not work through the motor capacity to the bearing.

4.1.1 Frequency components in the potential equalization system

Measurements at the frequency converter show in Figure ***4-1*** that the common mode current (*I CM*) is of particularly high frequency. It has significant powerful signals up to 450 kHz under strong interfering variable influence at the example of a 335 kW drive. Consequently, the frequencies of the same mesh on the return path through the motor cable shield (*I S*) are nearly identical. Signals with very low amplitude level can be detected up to 1.2 MHz. In the investigation of 50 drive trains in the field no significant powerful frequencies in the MHz range could be found. The common mode voltage is significant only up to 100 kHz and is much more low-frequent than the common-mode current.

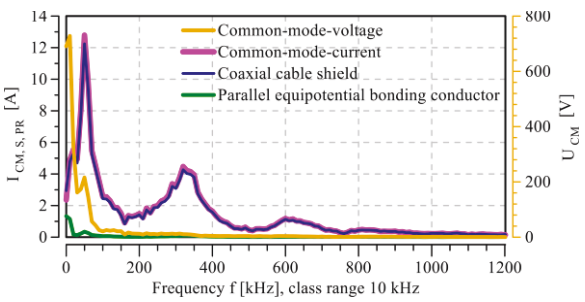

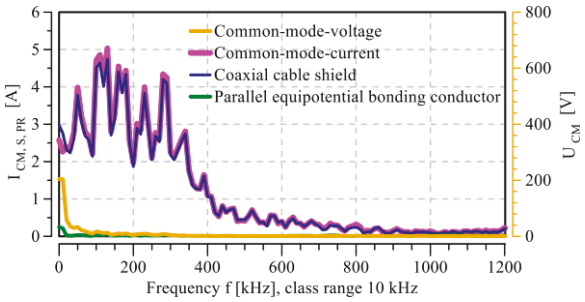

Figure 4-1*: Frequency spectrum on the frequency converter, 335 kW drive, 690 V, frequency control 2.5 kHz, controlled infeed, strong disturbance factors (left)*

Figure 4-2*: Frequency spectrum on the frequency converter, 1150 kW drive, 690 V, frequency control 2.5 kHz, uncontrolled infeed, average disturbance factors (right)*

Very interesting, as yet rarely studied, are the frequencies on the parallel bonding conductor (*I PR*), which returns from the motor base on a direct path to the frequency converter. Especially

the frequencies in the low-frequency range below 1 kHz characterize the current. Significantly in the milliampere range this current is up to 100 kHz although the drive train is exposed to many disturbance factors.

The same measurement on a considerably larger 1150 kW drive under medium disturbance factors shows significantly lower high-frequency amplitudes in all the signals (Figure ***4-2***). The drive train is in this case supplied by an uncontrolled infeed.

Because of the uncontrolled infeed the high amplitudes in the range of 50 to 100 kHz are missing as compared with the measurement at the 355 kW drive with controlled infeed. The common mode voltage is also significantly reduced in peak height.

The tests shows that the frequency spectrum of the signals measured here constitute an individual fingerprint of each drivetrain. The variance of the curves is also high with regard to almost identical drivetrains.

5 Common-mode currents during dynamic drive train operations

In practice, it can be observed again and again that drives at dynamic processes fails due to preterm bearing damages with multiple reasons. From [4] and [1] the rotational speed dependence of bearing currents is known. But it is important to know how the common mode current and how the regulation and the pulse pattern behave due to the very low motor velocities.

On a 90 kW drive, which is used as a multi-motor drive, different speeds were successively approached with continuous common mode current measurement.

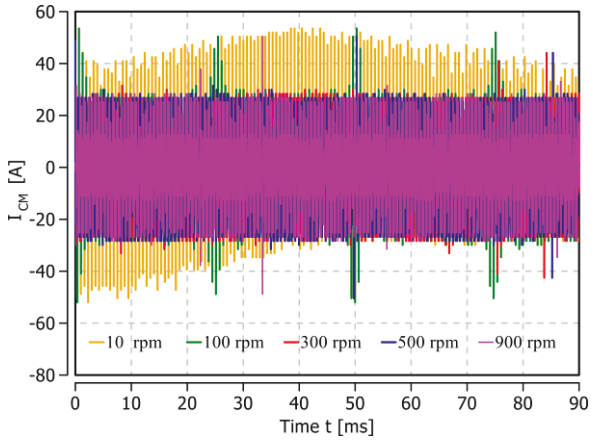

Figure 5-1*: Speed dependency of common mode current due to the frequency modulation. 90 kW drive, 400 V, uncontrolled infeed, low disturbance factors*

The Figure ***5-1*** shows the overlaying of these measurements at different rotational speeds from 10 rpm up to 900 rpm. Clearly noticeable is that the values for very low speeds are very different

from all other measurements. Ranging from 300 rpm to 900 rpm, the differences seem small and a stable high common peak level stands out in which at the amount of around 25 A_p particularly common mode peaks occur. This peak level can be explained by the step-like common-mode voltage. The voltage difference of the flanks is repeatedly the same size and thus also a repetitive equally large common-mode current flows. The number of particularly high peaks of the average peak level is much high at 10 rpm.

The histogram classification in Figure ***5-2*** shows the count of the measured common mode current peaks. The positive peaks were counted hiding the post oscillation which also exhibit maxima.

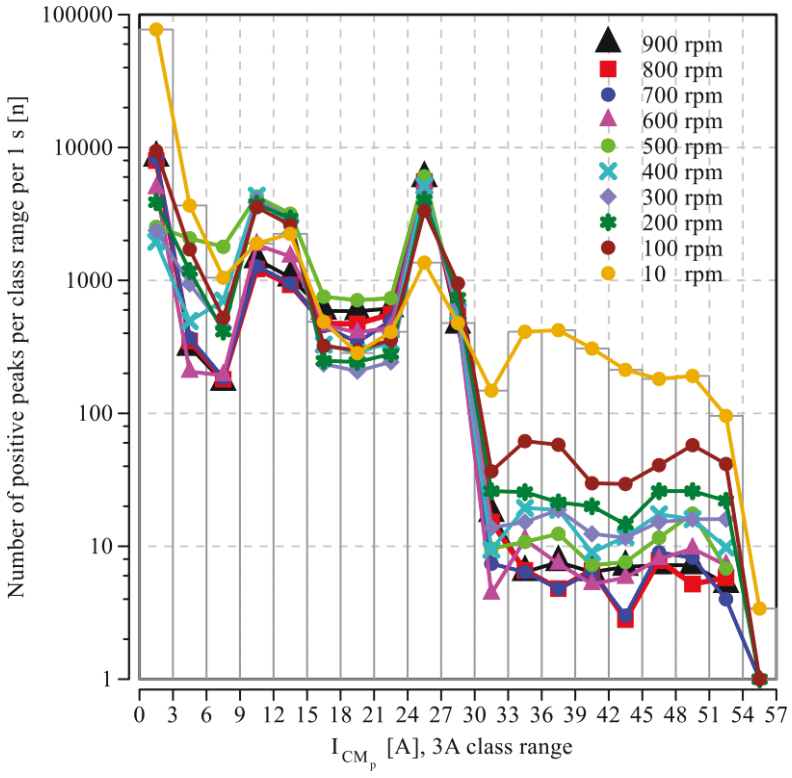

Figure 5-2*: Histogram analysis, counted common mode current peaks and power levels for different speeds, class width 3 A, 90 kW drive, 400 V, uncontrolled infeed, low disturbance factors*

The maximum peak heights lie across the speed in the range of 54-57 A_p. The trend shows that the number of high common mode current peaks increases with decrease in the speed. The number of high common-mode peaks lies for 10 rpm about 20-times above the comparable figure at speeds of 700 – 900 rpm. The most common mode current peaks can be found 3 A_p. Here peak frequencies up to 10,000 peaks per second and at low speeds (10 rpm) up to 80,000 peaks per second are counted.

With regard to the damage potential in the bearing especially the medium and high peak amplitudes due to higher energy levels are interesting.

Due to the modulation method of the frequency converter a strong increase in the number of peaks can be observed at 10 rpm. In order to produce a very low frequent motor phase current, more and more null pointer must be switched by the inverter which raises the common mode voltage to their absolute maxima and minima. With the result of high peak-shaped charge and discharge currents.

Three-dimensionally processed (Figure ***5-3***) a typical ridges and valley landscape shows for common mode currents which move largely in a constant to slightly sloping corridor with the exception of very low speeds. The lower (9-15 A_p) and medium (24-27 A_p) stable peak level occurs as a clearly recognizable back.

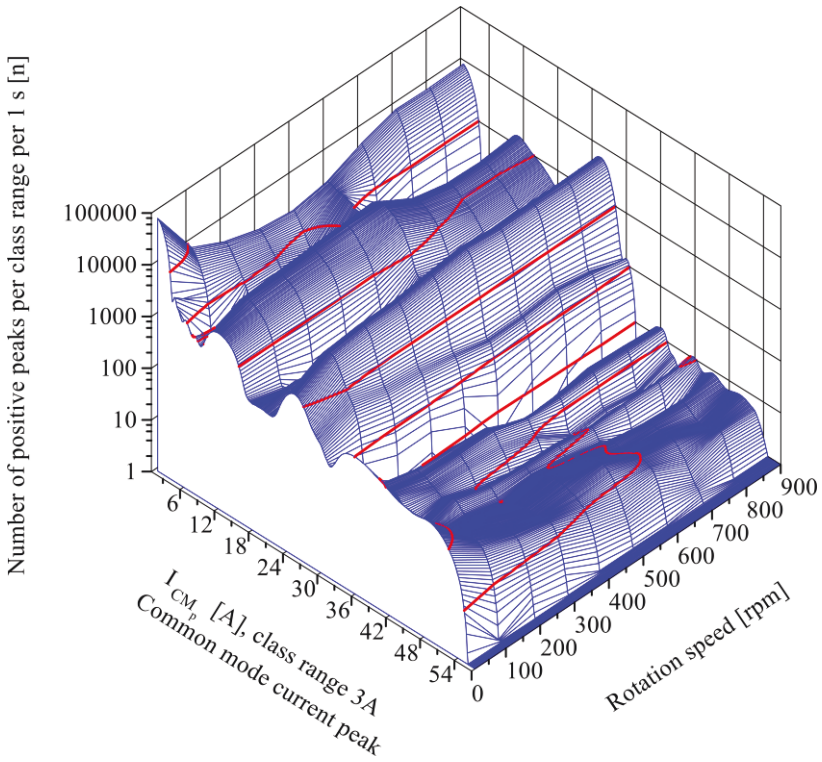

Figure 5-3*: Histogram analysis, areal representation of the common-mode current number of peaks and current levels as a function of the rotational speeds, class width 3 A, 90 kW drive, 400 V, uncontrolled infeed, low disturbance factors*

6 Nanocrystalline tape wound cores for reducing bearing currents

Reduction of bearing currents can be successfully done in different ways. Following a procedure which is in practice still rarely applied will be examined: the use of nanocrystalline tape wound cores in the motor feeder area. This countermeasure is also suitable for retrofitting to

existing installations. The tape wound cores act as common mode choke and damp the common mode current flow. Thereby, the bearing current can be reduced. The tape wound cores are attached to the motor phases without bonding conductor and motor cable screen.

By the nanocrystalline properties of the material, a relatively thin core can be constructed, which has a particularly low power loss (4 W/kg material at 20 kHz and 200 mT) at a high saturation inductance (1200 mT) and high permeability [13], [14]. The cores, which are attached to the insulated outer conductor, must not damage the conductor insulation thermally. Often the mounting space between the cable support rail in the inverter and the connection to the output terminal (mostly bus bar connections at large scale inverters) is very limited. In order to achieve the necessary damping at low heating of the tape wound cores, it can be necessary to use multiple cores in series. Figure ***6-1*** shows the installation in an existing drive. There 3 cores are installed above each other.

Figure 6-1*: Installed nanocrystalline tape wound cores to reduce common mode currents in the main field of a large inverter, three tape wound cores installed above each other.*

6.1.1 Influence of nanocrystalline tape wound cores to the common mode current

As part of a large comparison study of over 50 drive trains the efficacy of nanocrystalline tape wound cores was investigated. It can be seen due to the interference and influences that each drive train shows different efficiencies of tape wound cores. Despite these differences, many measurements follow similar results.

The example of a 690 kW drive train clarifies the study's main results, see Figure ***6-2***, Figure ***6-3*** and Figure ***6-4***.

All measurements were taken in succession once with disabled tape wound cores and once with activated tape wound cores. Without nanocrystalline tape wound cores the maximum peak common mode current (I_{CM}) was 145.2 A_p. With activation of the tape wound cores the value dropped drastically to maximum 99.5 A_p. This change represents a reduction of 31 %. Looking at the upper stationary peak level an even greater reduction is observable. Without cores this level is 74 A_p, with active tape wound cores at 26 A_p. This corresponds to a reduction of the upper stationary peak levels by 65 %.

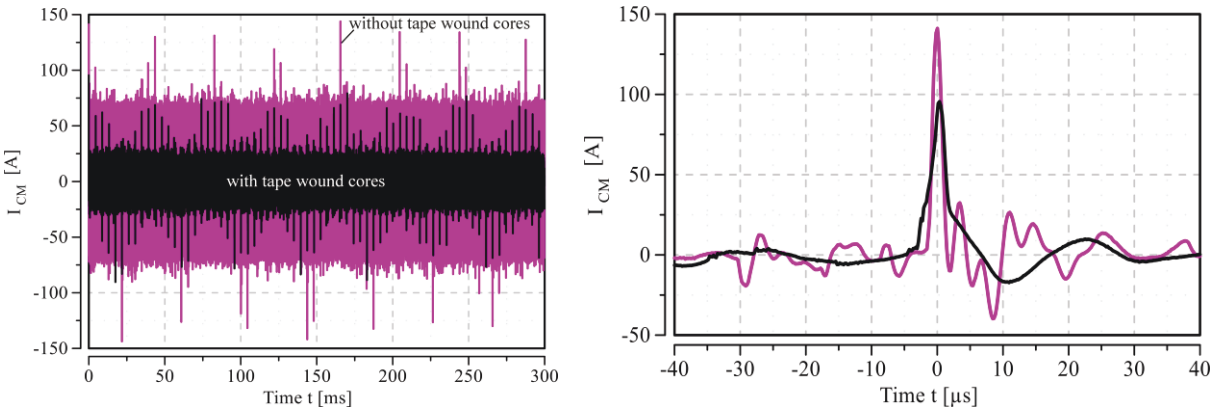

Figure 6-2*: Measurement of common mode current (I_{CM}) with and without nanocrystalline tape wound cores, 690 kW, 690 V, multi-motor drivetrain (left)*

Figure 6-3*: Comparison of single peaks of common mode current (I_{CM}) with (black) and without (purple) nanocrystalline tape wound cores, 690 kW, 690 V, multi-motor drivetrain (right)*

Looking at the highest measured common mode current peak in Figure ***6-3*** especially the absorption and smoothing is significant. The very typical oscillation after the peak is limited by tape wound cores. The black line has an almost aperiodic shape (black curve). Small peaks are almost completely damped with tape wound cores.

6.1.2 Influence of nanocrystalline tape wound cores on the common-mode voltage and equipotential bonding

For the common-mode voltage (U_{CM}) can be stated that this is only slightly affected by the tape wound cores (Figure ***6-4***). The signal shape and height remains almost the same. A slight increase in the common-mode voltage can be shown due to the damping of the common mode

current. The loop impedance rises to compensate for the common mode voltage. The voltage source is thus less stressed.

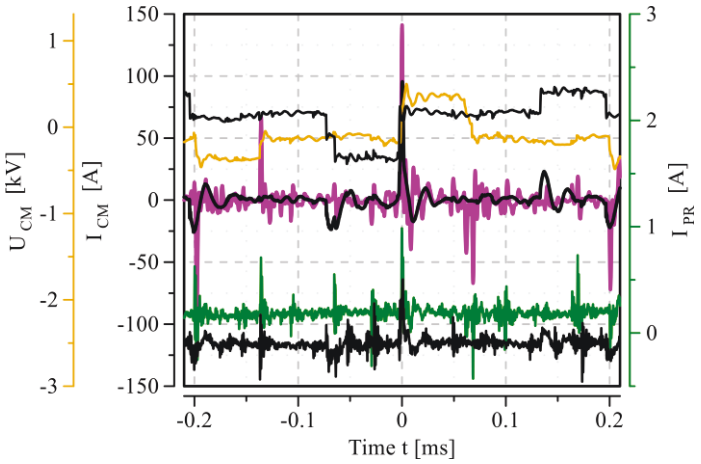

***Figure 6-4**: Comparative measurement with and without nanocrystalline tape wound cores. The respective black curve corresponds to the value with active tape wound cores 690 kW, 690 V, multi-motor drivetrain*

As in Chapter 4 described, at a low impedance potential compensation system only a small fraction of the common mode current flows through the parallel bonding conductor of the motor cable (parallel return conductor) back through that path to the frequency converter. Over this track even unbalanced currents in the fundamental frequency range below 1 kHz flow which are not directly related to the common mode current. The common mode current overlays on this basic wave. Consequently, the parallel return current (I_{PR}) is expected to be less changed using tape wound cores. This is also confirmed by the measurements in Figure ***6-4***. The peaks of the parallel return conductor current appear only slightly changed in shape and signal level by the cores. The changed fundamental level results from the described low fundamental frequencies of the signal. A slight reduction of high-frequency small peaks on the signal can be seen.

6.1.3 Reduction of high-frequency parts by nanocrystalline tape wound cores

With Fast Fourier Transformation (FFT) the respective frequency responses of the peak amplitudes have been determined. Figure ***6-5*** shows the frequency spectrum for common-mode currents and parallel return line currents in comparison with and without tape wound cores. A class width of 10 kHz was used for the evaluation, because the high-frequency peak signals are usually in a frequency band and do not hit any accurate frequency repeated.

Without tape wound cores the FFT of the 690 kW drive shows significant frequencies of common mode current up to 500 kHz. The common mode current is presented with very high frequency. Particularly high peak amplitudes are observed in the frequency intervals at 80, notice 180 and 280 kHz. The parallel return conductor current is mainly characterized by fundamental frequencies below 1 kHz and by frequencies up to 20 kHz. Significant signals increases can be observed in the range of 750 kHz to 1200 kHz. It is clearly seen that this frequency range is not present in the common mode current signal. Thus, this current cannot be directly causal. Rather, similarities to the frequencies of the rotor ground current can be found which are suitable for this high-frequency signal rise in the parallel return line. Because of the low peak amplitude of less than 40 mA per 10 kHz interval, and thus low power, no further actions in the equipotential bonding system are considered to balance these currents.

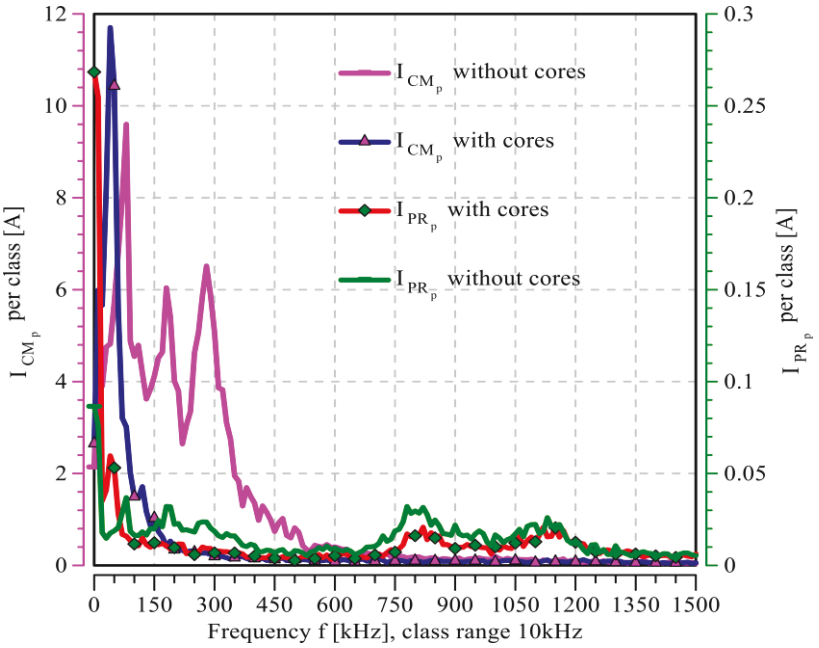

***Figure 6-5**: FFT of the signal components of common mode current ($I_{CM\,p}$) and parallel return conductor current ($I_{PR\,p}$) with and without tape wound cores, class width 10kHz, Hamming window, 690 kW, 690 V, multi-motor drive-train*

6.1.4 Change of number and amplitude of the common mode current peaks by tape wound cores

The damage in the rolling bearing are dependent on the frequency of rollovers and cratering in the bearing runway. To determine the number of peaks in the common-mode current a corresponding algorithm was programmed which only counts the common mode current peaks

caused by the common-mode voltage variation. This is important to hide the amplitude maxima of the oscillating waves of the common mode current since they would distort the count.

In Figure ***6-6*** the peak numbers of a 690 kW drive train with and without nanocrystalline tape wound cores are compared. In addition to the significant reduction of the overall number of peaks, the number of peaks with particularly large amplitudes greater than 30 A is reduced by the tape wound cores.

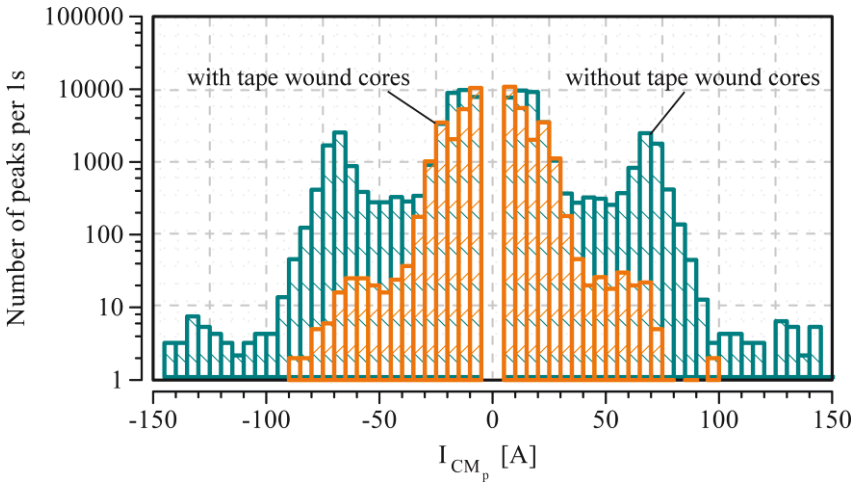

Figure 6-6*: Histogram count of peak amplitudes of common mode current (I_{CMp}) with (orange) or without (turquoise) tape wound cores, class width 5 A, 690 kW, 690 V, multi-motor drivetrain*

7 Conclusions

The studies under field conditions have provided a variety of exciting insights in dealing with bearing damage. The following aspects may be mentioned here in the first place:

- Under industrial interfering variable influence the common mode voltage is severely distorted until the typical step shape of the signal is hardly detectable.
- A strong influence on the form and peak level of common-mode currents has the choice of infeed technology of the frequency converter. Uncontrolled infeed seem advantageous in terms of lower bearing currents in the investigated examples.
- For a correct and low impedance equipotential bonding system with coaxial shielded symmetrical motor connecting cable more than 95 % of the common mode current flows back via the motor cable shield to the frequency converter.
- A particularly low impedance motor cable shielding is therefore recommended.

- The common mode current in the studies is significant in the frequency range up to 500 kHz and therefore very high-frequent. Weak signals are detected to 1.2 MHz.
- At low impedance motor cable shields the high-frequency common-mode currents flow back only very slightly on other ways as parallel return line, foundation earth, ring earth and motor shaft and rotor ground current.
- The powerful frequencies on this other bonding conductor are present to a maximum of 20 kHz. Current components below 1000 Hz clearly dominate. Weak signals are detected up to 1.2 MHz.
- The use of special for the "EMC" exchange optimized superfine parallel return conductors is questionable at this frequency range.
- From the viewpoint of bearing currents an additional parallel to the motor cable bonding conductor can be leaved away.
- The maximum peak height and peak number of the common mode current is only of low impact by speed on a wide speed range At very low speeds the peak frequency may increase by a factor of 20 since the converter has to switch null pointer.
- By installing nanocrystalline tape wound cores the potential of harmful bearing currents can clearly be reduced. The tape wound cores damp the common-mode current. The individual common mode current peak amplitudes and stationary peak level heights have been reduced strongly. Especially higher-frequency components are significantly reduced.
- Also tape wound cores have a positive effect on the number of common-mode peaks.

8 References

[1] A. Mütze, *Bearing currents in inverter-fed AC-motors*. Zugl.: Darmstadt, Techn. Univ., Diss., 2004. Aachen: Shaker, 2004.

[2] K. Sommer, R. Heinz, and J. Schöfer, *Verschleiß metallischer Werkstoffe: Erscheinungsformen sicher beurteilen,* 3rd ed. Wiesbaden: Springer Fachmedien Wiesbaden, 2018.

[3] E. C. Wittek, “Charakterisierung des Schmierungszustandes im Rillenkugellager mit dem kapazitiven Messverfahren,” Dissertation, Leibniz Universität Hannover, Hannover, 2016.

[4] H. Tischmacher, “Systemanalysen zur elektrischen Belastung von Wälzlagern bei umrichtergespeisten Elektromotoren,” Dissertation, Hannover, 2017.

[5] A. Mütze and A. Binder, *Elektrische Lagerbeanspruchung bei umrichtergespeisten Maschinen: Abschlussbericht*, Darmstadt, 2003.

[6] A. Furtmann and G. Poll, “Electrical stress and parasitic currents in machine elements of drive trains with voltage source inverters,” in *International Conference on Gears 2017*, pp. 109–118.

[7] V. Hausberg and H. O. Seinsch, “Wellenspannungen und zirkulierende Lagerströme bei umrichtergespeisten Induktionsmaschinen | Shaft voltages and circulating bearing currents of converter supplied induction machines,” (ger), *Electrical Engineering: Archiv für Elektrotechnik*, Vol. 82, No. 6, pp. 313–326, 2000.

[8] V. Hausberg and H. O. Seinsch, “Kapazitive Lagerspannungen und -ströme bei umrichtergespeisten Induktionsmaschinen,” (eng), *Electrical engineering: Archiv für Elektrotechnik ; research journal*, Vol. 82, pp. 153–162, 2000.

[9] Y. Gemeinder, “Lagerimpedanz und Lagerschädigung bei Stromdurchgang in umrichtergespeisten elektrischen Maschinen,” Dissertation, 2016.Bonn

[10] B. Radnai, “Wirkmechanismen bei spannungsbeaufschlagten Wälzlagern,” Dissertation, Technische Universität Kaiserslautern, 2016.

[11] A. Ruf, F. Pauli, M. Schröder, and K. Hameyer, “Lebensdauermodellierung von nichtteilentladungsresistenten Isoliersystemen elektrischer Maschinen in dynamischen Lastkollektiven,” *e & i Elektrotechnik und Informationstechnik*, Vol. 135, No. 2, pp. 131–144, 2018.

[12] J. Specovius, *Grundkurs Leistungselektronik: Bauelemente, Schaltungen und Systeme,* 8th ed. Wiesbaden: Springer Vieweg, 2017.

[13] MAGNETEC GmbH, *Typische Werkstoffkennlinien von NANOPERM*. Langenselbold, Germany. Accessed on: May 11 2018.

[14] MAGNETEC GmbH, *Vergleich weichmagnetischer Werkstoffe.doc*. Langenselbold, Germany. Accessed on: May 11 2018.